Armenian Journal of Physics, 2009, vol. 2, issue 3, pp. 200-212

IMPROVEMENT AND STABILIZATION OF THIN-FILM HYDROGEN SENSORS PARAMETERS

A.Z. Adamyan[1], Z.N. Adamyan[1], V.M. Aroutiounian[1], K.D. Schierbaum[2], S-D. Han[3]

[1]*Department of Physics of Semiconductors and Microelectronics; Center of Semiconductor Devices and Nanotechnologies at Yerevan State University, 1, A.Manoogian, 0025, Yerevan, Armenia*

[2]*Department of Material Sciences at Institute for Condensed Material Physics, Heinrich-Heine University, Building 25.23, 1, Universitätsstr., D-40225, Dusseldorf, Germany*

[3]*Sensors & Material Research Center; Advanced Energy Materials & Application Research Department at Korea Institute of Energy Research, 71-2, Jang-dong, Yuseong-gu, Daejeon, 305-343, Korea*

PACS number: 07.07.Df

Abstract. The sol-gel derived thin-film SnO_2 hydrogen gas sensors sensitization and parameters stabilization by specific treatments methods are presented. It is established that presented annealing treatment regimes and initial operation mode leads to rise in the sensors sensitivity by more than two orders of magnitude, as well as to improvement of the sensor parameters stability in time. It is shown that stability of the sensors parameters remains also under long-term operation of the sensors in high humidity conditions. Obtained experimental data are in good accordance with known theoretical results.

Keywords: SnO_2; Hydrogen sensor; Nanocrystallites; Thin film; Gas sensitivity; Humidity.

Introduction

Production requirements and interest of researches groups for high sensitive, selective, reproducible, reliable, and stable hydrogen sensors has been growing steadily [1-3]. This is first of all related with necessity of using hydrogen sensors in such rapidly developed fields of applications as fuel cells including for motor car construction [3], atomic and thermal power stations [4, 5], cosmic researches [6], etc.

Metal-oxide hydrogen sensors in comparison with other types of the sensors such as: catalytic [7], electrochemical [8], thermoelectric [9], have a number of advantages. Amongst them, it should be noted the low threshold of sensitivity, small sizes, low price, large temperature range of reliable sensor operation, compatibility with state-of-the-art microelectronic technology allowing one to set on foot large-scale production of such sensors.

Disadvantages of the metal-oxide sensors are relatively low accuracy of measurements of the affecting hydrogen concentration, dependence of sensors' parameters on temperature, ambient humidity and their insufficient stability in time. We have succeeded to overcome some of these shortcomings, in particular, for example, humidity dependence [10-13], by using pulse heating of the sensors at a certain frequency which ensures the regeneration of semiconductor film surface.

We believe that one of principal causes of instability of sensor parameters is conditioned by the growth of nanocrystalline grains at raised operating temperature. However, sol-gel derived SnO_2 thin-film hydrogen sensors technology developed by us ensures a relative stability of grain size with the rise of temperature [10-12]. Moreover, the operating temperature of developed sensors is low enough (not exceeding 150^{o}C) [12-14]. This means that we have succeeded to particularly improve the stability of sensors parameters. Nevertheless, some instability of the sensor characteristics exists so far, and this is one of main causes preventing extensive use of such thin-film metal-oxide gas sensors in practice.

The results of our efforts devoted to find the ways for in-time stabilization of developed sol-gel derived SnO_2 thin-film hydrogen sensor parameters are presented below.

Experimental

The samples of tin dioxide thin-film sensors were obtained by the sol-gel technique presented in detail elsewhere [10-12]. The sol solution was spin-coated at 3500 rpm on thoroughly cleaned alumina substrate with previously formed Ti/Pt interdigitated electrodes. Thin Ti sublayer and Pt film were sequentially deposited on the substrate using e-beam evaporation. The spin coating procedure was repeated 6 times, with 450^{o}C annealing during 1 hour after each layer deposition. The rate of temperature rise from 20 to 450^{o}C was maintained at the value of 1^{o}C/min. The final annealing with already deposited sixth layer was made at 650^{o}C for 2 hours.

Upper thin catalytic Pt layer was deposited on the samples by also e-beam evaporation. The e-beam evaporation was made on the substrate heated up to 150^{o}C. Average thickness of the deposited film was controlled with a quartz resonator and was evaluated at the value 20 nm with average deposition speed of ~0.6 Å/sec. The pressure in the vacuum chamber was $7\cdot10^{-6}$ Torr before starting the evaporation process and $1.5\cdot10^{-5}$ Torr during the process.

As a result, the sol–gel derived tin oxide thin films with 100–120 nm thicknesses were obtained. Thickness of the studied films was determined from reflectance spectra as well as using of the Stylus Profiler Ambios XP-1 profilometer. The SnO_2 thin films obtained by such a way were studied by us earlier using TEM, SEM and STM microscopy [10, 11, 13, 14]. Analysis of obtained images was revealed that the nanocrystallites sizes did not exceed 10 nm even after the calcinations at 750 ^{o}C.

After deposition of the catalytic layer, the final annealing was performed in air according to the program presented in Table 1.

After deposition of the catalytic layer, the final annealing was performed in air according to the program presented in Table 1. The temperature of final annealing was selected higher than the

temperatures of previous annealing processes with sol-gel layers as it is known [16] that at 700–750 ^{o}C temperatures the recrystallisation of sputtered or evaporated Pt catalyst layer occurs.

Table 1. Thin-film hydrogen sensors annealing treatment program steps.

Temperature change interval, ^{o}C	Temperature rise rate, ^{o}C/min	Hold time after the end of interval, min
20-470	5	0
470-650	1	150
650-750	2	0
Refrigeration along with furnace cooling down		

This leads to formation of Pt nanoclusters covering the sensitive layer which apparently significantly increases the catalytic activity of Pt layer and, hence, to increase in gas sensitivity and lowering of sensor operation temperature.

The measurements of sensor parameters were conducted on two automated software-controlled measurement setups:

1. The measurements of the thin-film hydrogen sensors parameters were carried out using the PC-controlled automated measurement setup which allows in situ monitoring and recording the change in the sensor characteristics and parameters depending on gas concentration and operation temperature. Simultaneously, by means of the developed automated measurement setup, it is possible to register the change of gas sensor temperature as well as the temperature and pressure of the environment in the chamber during measurements. The developed by us measurement system software control allows us displaying changes in sensor resistance caused by rapid adsorption–desorption processes as well as long-term sensor resistance changes connected with ageing or stabilization of the parameters over a long period of time. The developed by us PC-controlled, automated measurement setup arrangement, circuit design and full measurement capabilities are presented elsewhere [12, 13, 17].
2. Hydrogen sensors parameters testing at its operation under simultaneous action of various concentrations of hydrogen/air mixture and different surroundings RH were carried out on the base of automated setup under constant gas mixture flow rate of 50 sccm. The setup allowed adjusting RH and gas concentration in time according to predetermined program.

Results and discussion

The measurements of the hydrogen gas sensitivity to 1000ppm H_2 as well as 90% response and recovery times at different operation temperatures were carried out for both as-prepared and aged sensors. The measurements results for as-prepared sensors are presented in Table 2.

Table 2. As-prepared hydrogen sensor sensitivity and reaction kinetics versus operating temperature.

T, °C / Sensor parameter	90	110	130	150
90% responce time, s	450	40	7	2
90% recovery time, s	100	52	20	20
$S_{1000ppm}$, R_{air}/R_{gas}	50	45	30	50

Hereinafter, *S* is gas sensitivity expressed as the ratio of electrical resistance in air (R_{air}) to that in the sample gas (R_{gas}); subscript with S (1000, 5000, etc.) indicates the tested gas concentration in ppm.

It should be noted that the above-mentioned parameters are not well reproducible in the case of as-prepared sensors. In order to stabilize the sensitivity and time performance of the sol-gel derived thin-film hydrogen sensors, we have carried out special relatively long-term ageing of the as-prepared samples in air with 0.5% hydrogen at 150°C with continuous measurements of the sensor resistance changes. The results are presented in Fig. 1 and 2.

As a first step of the stabilization ageing, the as-prepared samples of thin-film hydrogen sensors were placed in the measurement chamber under standby state conditions in air at operating temperature (150°C). After such ageing during a few days we made sure that sensor's parameters did not change in time. Further, as a result of initial inlet of 1000 and 5000ppm hydrogen into the chamber, relatively low sensitivity (S_{1000}=5 и S_{5000}=100) was observed. At 1000 ppm hydrogen action, the sensor resistance at first drops as shown in Fig. 1 and then after some rise settles at a constant value. We can also note that the sensor operation is entailed with significant increase in its substrate temperature (dotted line in Fig. 1) despite of, as our corresponding measurements have shown, the power consumption of the sensors still remains constant. This fact indicates about catalytic exothermic reaction of hydrogen oxidation on sensor surface. Following temperature decay which takes place simultaneously with sensor resistance rise (1000–7000 s regions in Fig. 1), is conditioned by consumption of hydrogen in the chamber, so the concentration of H_2 in the chamber decreases. Numerical evaluation of the heat balance also points to the fact that additional heating of the sensor takes place namely owing to the hydrogen oxidation.

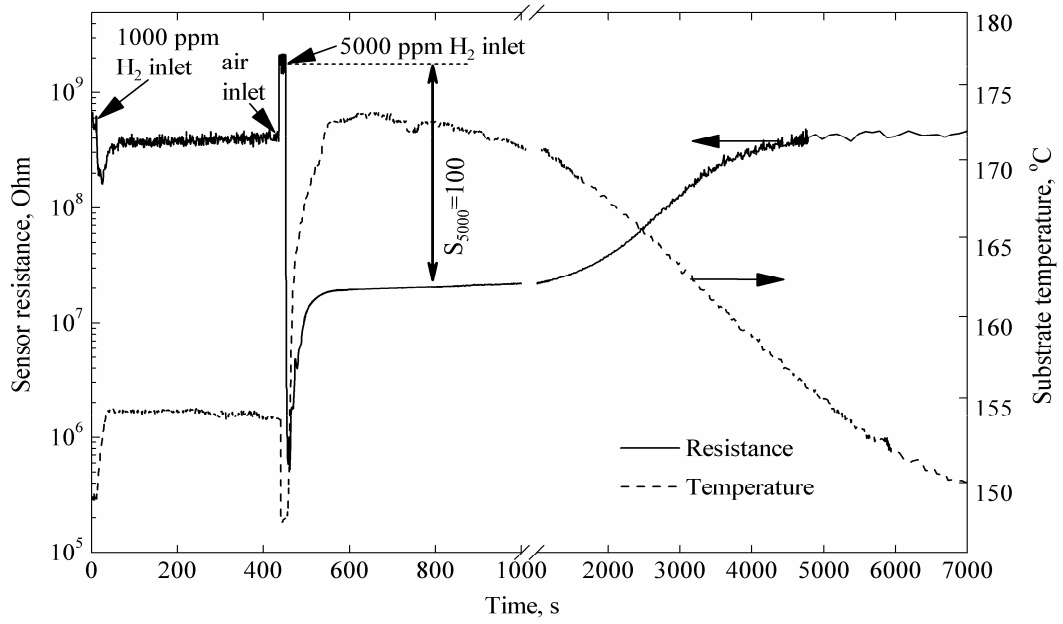

Fig. 1. Plots of hydrogen sensor resistance and substrate temperature with time in initial stage of the long-term treatment.

After proper air blowing of the chamber, during the next H_2 inlet, this process runs again (0–0.8 day region in Fig. 2). This procedure of chamber air blowing and inletting hydrogen with same concentration was repeated several times. Analyzing the results of this long-term ageing and testing shown in Fig. 2, we can conclude that the catalytic combustion rate decreases in the course of time, reaching almost zero after fifth day (sensor response and H_2 concentration in the chamber remains constant at that). Nevertheless, the described process of sensors ageing is accompanied with sensor sensitivity rise up to $S=2\cdot10^4$ to the end of the ageing process mainly due to decrease in the R_{gas} value and holds out during the further sensors operations.

The measurement of response and recovery times immediately after the ageing shows that the long-term exposure under hydrogen-containing atmosphere leads to some slowing of sensor reaction. The similar effect is observed when the sensors were placed in air during a long time. However, this effect disappears after short-term exposure to hydrogen/air mixture in the operation conditions or short (10 min) heating up to 300°C. Finally, after fulfillment of these procedures, sensor reaction data, for example, under effect of 1000 ppm hydrogen and its removal are stabilized on the levels presented in Table 3. Definitive data of the sensors' reaction kinetic and gas sensitivity obtained by influence of different hydrogen concentration have an enough good reliability and reproducibility.

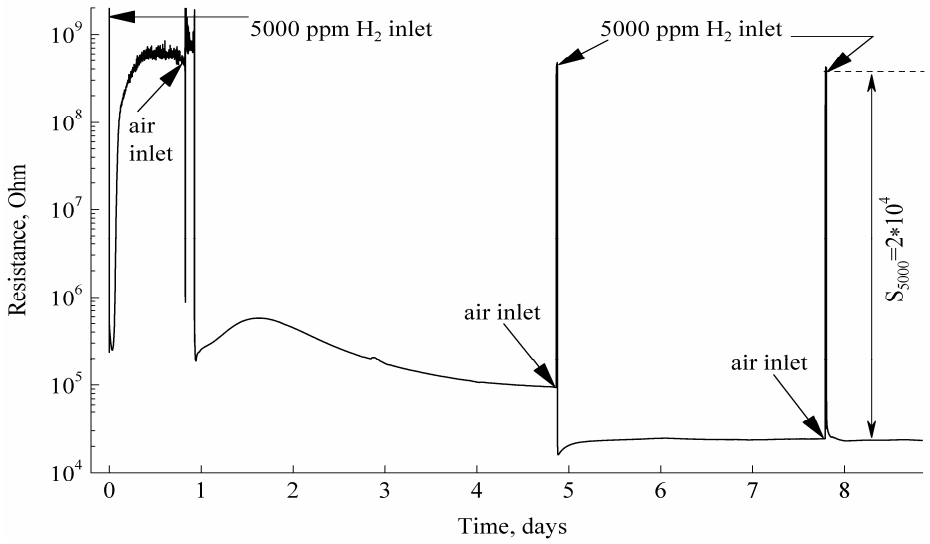

Fig. 2. Hydrogen sensor resistance changes during long-term exposure in hydrogen containing environment at operation conditions.

Table 3. The sensor parameters values depending on different operating temperatures after long-term treatment.

T, °C / Sensor parameter	90	110	130	150	170	190	220
90% responce time	150	120	95	15	12	11	6
90% recovery time	140	115	70	40	33	28	20
$S_{1000ppm}$, R_{air}/R_{gas}	150	300	1000	2000	1800	1800	1650

In order to measure sensor parameters, sensor operation temperature was firstly set at each level, and then hydrogen gas was injected into the chamber controlled to make a hydrogen/air mixture with desired gas concentration. An example of these measurements for one temperature point (150°C) is presented in Fig. 3.

It can be seen from Fig. 3 that during the first influence of hydrogen/air mixture, the resistance drops slowly (I part of the curve) in accordance with the equation

$$R = R_0 + A_1 e^{-\frac{t}{\tau_1}} + A_2 e^{-\frac{t}{\tau_2}}, \qquad (1)$$

Where R_0 and $R_0 + A_1 + A_2$ are sensor resistances at the end of I part of the curve, and during steady state in air, respectively; t is the time counted from the moment of test gas inlet into the measurement chamber, τ_1 and τ_2 are characteristic times.

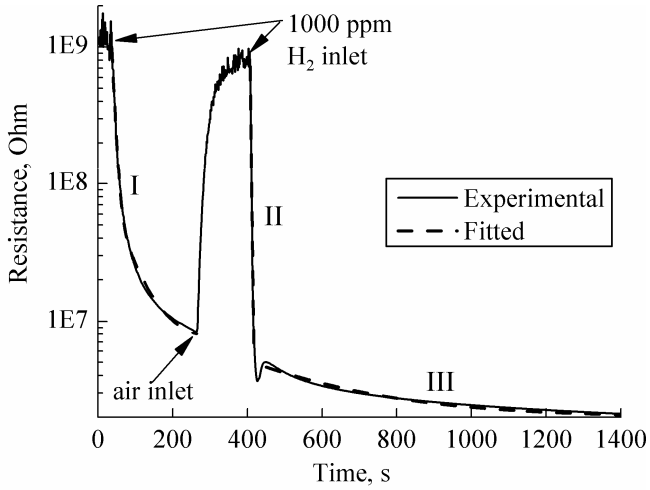

Fig. 3. Transients of sensor response to 1000 ppm H_2 and recovery in air (at 150°C operating temperature).

Then, after air blowing of the chamber, the repeated exposure to mixture with the same hydrogen concentration results in considerably faster sensor reaction (II part of the curve), followed by slow decrease tending to saturation (III part of the curve). Fitted dependences of the sensor resistance drop with time are plotted with dash line and coincide well with experimental data (solid line). The fitted curves related to II and III parts of the curve are in accordance with presented below equation (2) with different parameter values for each part:

$$R = R_0 + A_1 e^{-\frac{t}{\tau_1}} \tag{2}$$

Parameter values for each of equations (1) and (2) describing corresponding part of curve are presented in Table 4.

A result similar to equation (2), but for the concentration of adsorbed molecules, was obtained in theory [18] by solution of the kinetic equation describing the rate of change of concentration of molecules adsorbed on semiconductor surface in the case of nondissociative adsorption, namely:

$$N_b(t) = N_{bc}\left(1 - e^{t/\tau_a}\right). \tag{3}$$

Here, $N_b(t)$ and N_{bc} are the reducing gas molecule concentrations for the cases of non-dissociative adsorption and activated dissociative adsorption, respectively; τ_a is the relaxation time for the adsorption process.

Table 4. Values of different parameters appearing in Eqs. 1 and 2 for each of part of R(T) curve presented in Fig. 3.

Part of curve in Fig.3 \ Parameter	A_1, Ohm	A_2, Ohm	τ_1, s	τ_2, s	R_0, Ohm
I (Eq. 1)	$1\cdot10^9$	$6.2\cdot10^7$	7.1	54.2	$7.1\cdot10^6$
II (Eq. 2)	$7.2\cdot10^8$	—	2	—	$2\cdot10^6$
III (Eq. 2)	$2.6\cdot10^6$	—	280	—	$2\cdot10^6$

Analysis of SEM, TEM and STM images [10, 11, 13] has shown that the tin dioxide films studied by us are porous structures consisting of SnO_2 nanocrystallites or grains. Oxygen from air adsorbs on the surface of these nanocrystallites, captures there electrons from conduction band of SnO_2 and consecutively turns into negatively charged ions. This leads to electron-depleted layer formation and surface potential increase. The nanocrystallites are connected with each other either immediately, through grain-boundaries forming the so-called double Schottky barrier, or through narrow bridges – necks of the same material [19]. The electric contacts of the sensor are connected with chains formed by such structural units. In porous SnO_2 films gas environment affects the electric conductivity of all nanocrystallites and necks. This fact should be taken into account when considering both the sensors sensitivity mechanisms and kinetics of interaction between gas particles and surface states. As shown in [18, 20], the thickness of the conductivity necks is about 10 times smaller than cross-cut sizes of the nanocrystallites. In this case, as indicated in [18-21], the size of the nanocrystallites plays a vital role. This means that the conductivity of nanocrystallites chains is mainly determined by necks resistances with dimensions of the nanocrystallites close to the Debye length. At the grains size smaller than the Debye length, nanocrystallites are entirely carrier-depleted, so the resistance is determined by double Schottky barrier at the grain boundaries.

The operating temperature of developed hydrogen sensors (150^oC), revealed by sensitivity measurements at different temperatures, coincides completely with the transition temperature [22] at which some kind surface states are interchanged with others. It is known [22, 23] that below the mentioned temperature, oxygen is mainly adsorbed as O_2^- while at 160^oC and above the O_2^- states are transformed into O^- ($2O^-$) and then into O^{2-}. Thereafter, additional free electrons are captured by these new surface states. As a result, the height of the Schottky barrier on the grain boundaries and hence the sensors resistance are increased.

It is also known [24] that water molecules which were located on the surface and covered the surface state active for chemisorption are entirely removed at 150^oC (although hydroxyl groups are desorbed beginning only from 250^oC). But this process is known [25] to occur slowly, at least far slower than the adsorption of H_2 and O_2. This fact explains the long reaction time at temperatures

lower than 150°C and, in particular, the increase in sensitivity with temperature rising till water molecules remove from chemisorption centers.

To understand the physicochemical processes taking place in SnO_2 gas sensors during their operation, it is very important to take into consideration the role of atomic scale surface defects, which are able to significantly influence the gas sensors response kinetics as well as their sensitivity and stability in time. So, it is established [26] that the much stronger oxygen adsorption occurs at the sites of bridging-oxygen vacancies on the (110) surface of SnO_2 with adsorption energy of up to 1.8 eV. In this case, one missing atom in the row of oxygen atoms creates an adsorption site different from the case when all oxygen atoms are missing. In the last case, tin atoms can accept the Sn^{2+} valence essentially without breaking bonds. However, in the case of single type of oxygen vacancies (taking into account that the main defects in SnO_2 are double ionized oxygen vacancies V_o^{2+} [27]) there exist by a single breaking bond between each pair neighboring tin atoms on the surface. Moreover, the molecules adsorbed on the oxygen vacancies can interreact with neighboring oxygen sites. Taking into account that adsorption of atoms takes place firstly on lattice defects [24, 27, 28], including oxygen vacancies, it can be presumed that the local fields of defects impede the oxygen adsorption on the regular atoms of the surface by the change of the surface energy spectrum. Reaction of the oxygen and hydrogen atoms in this case will predominantly take place on the defects.

On the other hand, it is known that charged particles adsorbed on the film surface drift to anode in the applied electric field. In the anode region they eventually discharge electrons deep into the film or the contact and then are desorbed. Simultaneously the field in the defect surrounding is weakened, and the rate of oxygen adsorption on the lattice atoms is increased. The space charge region near the surface is increased owing to electron capture from the SnO_2 conductance band; hence, the sensing structure resistance is increased. Taking into account that charged oxygen vacancies and defects (including those of non-adsorptive origin) drift rather slowly, we can conclude that other processes associated with it are also slow. In fact, the stabilization of parameters takes place after five days of continuous working at the 150°C operation temperature under 5000 ppm hydrogen containing atmosphere (Fig.2). The presence of hydrogen in the chamber and its chemisorption on the lattice atoms lower the surface charge level. This leads to the reduction of the band bending which promotes the propagation of defects into the volume of semiconductor particle (in case of small nanocrystallites size in the range of double Debye length – into the space charge region). As a result, the probability of oxygen adsorption on the defects during subsequent sensor operation diminishes.

This can also explain the memory effect observed by us: after interruption of hydrogen influence and resuming it later (from a few hours up to 2 days) with the same concentration, the

sensor resistance drops faster to the value, at which hydrogen effect had been interrupted (short dotted line in Fig. 3). At a longer duration of stay in air, oxygen adsorption also on defects outlying of the surface can occur as a result of diffusion of oxygen atoms. Consequently, as a result of the first repeated hydrogen influence and participation of the defects in chemisorption reaction with return of electrons to the conduction band, the resistance drop occurs slowly (the sensor as if gets out unwillingly from the sleep mode). However, as it was mentioned above, the repeated influence leads to the fast reaction of the sensor (Fig. 3) because in this case preferably only lattice atoms being on the surface participate in chemisorption reaction. This leads to the change in the surface charge density, which influences practically immediately the width of space charge region. Assertion that at the fast sensor response only one type of centers takes part in the chemisorption reaction is confirmed by similarity of equations (2) and (3) as well as by the fact that the dependence (3) derived by taking into account only one type of adsorption centers [18, 20, 29].

After the definite long-term stabilization of the sensor operation and its sensitization was achieved, it was necessary to reveal the possibility of the sensors operation in much harsh environment, in particular, in high RH conditions. To that end, the corresponding research works were carried out. The results of these investigations are shown in Fig 4.

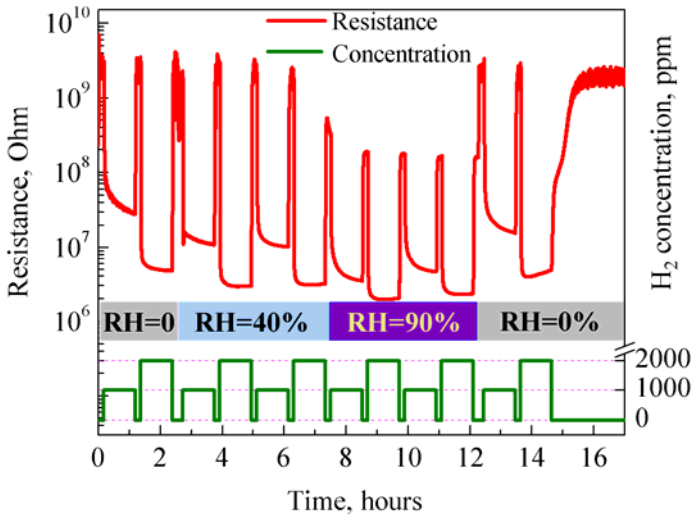

Fig. 4. Long-term testing of hydrogen sensor operation in different RH levels conditions.

As can seen from Fig.4, as would be expected in accordance with our previous works [12-14], the sensor sensitivity at low humidity levels (0-55% RH) remains practically constant. The sensitivity at higher RH levels slightly drops owing to decrease in sensor resistance in clean air. Nevertheless, the sensitivity remains enough high and, the most important, one does not change in time. Besides, we can note good reversibility of sensors operation. These facts offer the challenge

for application of studied by us hydrogen sensors in fuel cells, where hydrogen leakage sensors operate continuously in high humidity conditions (90% RH and higher).

Summary

Thus, presented sol-gel derived thin-film hydrogen sensors technological regimes and ageing conditions leads to both stabilization of the sensor parameters in time and to noticeable increase in hydrogen gas sensitivity (up to two orders of magnitude). At that, the response and recovery times in comparison with as-prepared samples were changed insignificantly.

The sensor sensitivity at operation in high humidity conditions remains enough high and does not change in time. Experimental date and fitted curves are in good agreement with known theoretical results. Taking into account of this fact, it is proposed the description of physicochemical processes occurring on the surface of the sensors in gaseous medium.

The good reversibility of sensors operation is also ensured.

We expect further improvement of the hydrogen sensor parameters, in particular reaction times, taking into account above-mentioned stabilization ageing, with application of silicon microhotplate platform (MEMS) device as a substrate for sensitive thin films, electrodes and heaters, as well as decreasing the inter-digital electrode finger spacing [30, 31].

Acknowledgments

This work was carried out in the framework of the ISTC 1232 project. Authors express their thanks to M. Elachhab for his help during testing of the sensors under various RH conditions.

REFERENCES

1. I.P. Jain, Hydrogen the fuel for 21st century, Int. J. of Hydrogen Energy 34 (2009) 7368–7378.
2. V.M. Aroutiounian, Metal oxide hydrogen, oxygen, and carbon monoxide sensors for hydrogen setups and cells, Int. J. of Hydrogen Energy, 32(9) (2007) 1145-1158.
3. V.M. Aroutiounian, Hydrogen detectors, Int. Sci. J. Alternative Energy and Ecology, 3(23) (2005) 21-31.
4. R. Loloee, B. Chorpening, S. Beer, R. Ghosh, Hydrogen monitoring for power plant applications using SiC sensors, Sensors and Actuators B 129(1) (2008) 200–210.
5. D. Kohl, Function and applications of gas sensors, J. Phys. D: Appl. Phys. 34 (2001) R125–R149.
6. G. Hunter, P. Neudeck, G. Jefferson, G. Madzsar, The development of hydrogen sensor technology at NASA Lewis research centre, NASA Technical Memorandum 106141, 1992.

7. L. Boon-Brett, J. Bousek, P. Moretto, Reliability of commercially available hydrogen sensors for detection of hydrogen at critical concentrations: Part II – selected sensor test results, Int. J. of Hydrogen Energy 34 (2009) 562-571.
8. L.P. Martin, A-Q. Pham, R.S. Glass, Electrochemical hydrogen sensor for safety monitoring, Solid State Ionics 175 (2004) 527–530.
9. M. Nishibori, W. Shin, N. Izu, T. Itoh, I. Matsubara, S. Yasuda, S. Ohtani, Robust hydrogen detection system with thermoelectric hydrogen sensor for hydrogen station application. J. Hydrogen Energy 34 (2009) 2834-2641.
10. A.Z. Adamyan, Z.N. Adamian, V.M. Aroutiounian, Preparation of SnO_2 films with thermally stable nanoparticles, Sensors, 3, 438-442, 2003.
11. A.Z. Adamyan, Z.N. Adamian and V.M. Aroutiounian, Sol-gel technologies for hydrogen sensitive thin film preparation, Int. Sci. J. for Alternative Energy and Ecology (ISJAEE) N 8(40) (2006) 24-30.
12. A.Z. Adamyan, Z.N. Adamian, V.M. Aroutiounian, A.H. Arakelyan, J. Turner, K. Touryan, Sol-Gel Derived Thin-film Semiconductor Hydrogen Gas Sensor, Int. J. of Hydrogen Energy v.32(16) (2007) 4101-4108.
13. A.Z. Adamyan, Z.N. Adamian, V.M. Aroutiounian, A.H. Arakelyan, Low-temperature high sensitive thin-film hydrogen sensor, Int. Sci. J. for Alternative Energy and Ecology (ISJAEE) N9(41) (2006) 11-16.
14. V.M. Aroutiounian, A.Z. Adamyan, Z.N. Adamyan, A.H. Arakelyan, Tin dioxide thin film hydrogen nanosensor, Proc. SPIE 6943 (2008) 69430J-1-69430J-12.
15. V.M. Aroutiounian, A.Z. Adamyan, Z.N. Adamyan, A.H. Arakelyan, Double-layer semiconductor gas-sensor advanced technology, Proc. VI Int. Conf. "Semiconductor Micro- and Nanoelectronics" (2007) 89-92.
16. J. Wöllenstein, H. Böttner, M. Jaegle, W.J. Becker, E..Wagner, Material properties and the influence of metallic catalysts at the surface of highly dense SnO_2 films, Sensors and Actuators B70 (2000) 196–202.
17. A.Z. Adamyan, Software-programmable setup for gas sensors parameters measurements, Izvestiya NAN RA and GIUA. Tekhnicheskie nauki LIX(1) (2006) 155–160.
18. I.A. Myasnikov, V.Ya. Soukharev, L.Yu.Koupriyanov, Semiconductor sensors in physicochemical researches, M. Nauka, 1991, 327.
19. N. Yamazoe, New approaches for improving semiconductor gas sensors, Sensors and Actuators B, 5 (1991) 7-19.

20. O.V. Anisimov, V.I. Gaman, N.K. Maksimova, S.M. Mazalov, E.V. Chernikov, Electrical and gas-sensitive properties of a resistive thin-film sensor based on tin dioxide, Semiconductors 40(6) (2006) 704-709.
21. C. Xu, J. Tamaki, N. Miura, N. Yamazoe, Grain size effects on gas sensitivity of porous SnO_2-based elements, Sens. Actuators B 3 (1991) 147–155.
22. S. Seal, S. Shukla, Nanocrystalline SnO gas sensor in view of surface reactions and modifications, JOM 54 (2002) 35–38.
23. S.C. Chang, Oxygen chemisorption on tin oxide: correlation between electrical conductivity and EPR measurements, J. Vac. Sci. Technol. 17 (1980) 366.
24. M. Batzill, U. Diebold, The surface and materials science of tin oxide, Progress in Surface Science 79 (2005) 47–154.
25. E.W. Thornton, P.G. Harrison, Tin oxide surfaces. Part 3.—Infrared study of the adsorption of some small organic molecules on tin (IV) oxide, J. Chem Soc. Faraday Trans. I 71 (1975) 2468.
26. F.F. Volkenstain, Electronic processes on the surface of the semiconductors under chemisorption, M., Nauka, 1987, 432.
27. J. Oviedo, M.J. Gillan, First-principles study of the interaction of oxygen with the SnO_2 (110) surface, Surf. Sci. 490 (2001) 221.
28. J. Mizusaki, H. Koinuma, J.I. Shimoyama, M. Kawasaki, K. Fueki, High temperature gravimetric study on nonstoichiometry and oxygen adsorption of SnO_2, J. Solid State Chem., 88 (1990) 443-450.
29. V.F. Kiselev, Surface phenomena in semiconductors and dielectrics, M., Nauka, 1970, 400.
30. C-H. Han, S-D. Han, I. Singh, T. Toupance, Micro-bead of nanocrystalline F-doped SnO_2 as a sensitive H_2 gas sensor, Sensors and Actuators B 109 (2005) 264–269.
31. S. Shukla, P. Zhang, H.J. Choa, S. Seal, L. Ludwig, Room temperature hydrogen response kinetics of nano-micro-integrated doped tin oxide sensor. Sensors and Actuators B 120 (2007) 573–583.